

Effect of Cr₂O₃ addition on oxidation induration and reduction swelling behavior of chromium-bearing vanadium titanomagnetite pellets with simulated coke oven gas

Wei-dong Tang¹⁾, Song-tao Yang²⁾, and Xiang-xin Xue¹⁾

1) School of Metallurgy, Northeastern University, Shenyang 110819, China

2) School of Materials and Metallurgy, University of Science and Technology Liaoning, Anshan 114051, China

(Received: 16 October 2018; revised: 20 January 2019; accepted: 28 February 2019)

Abstract: The oxidation induration and reduction swelling behavior of chromium-bearing vanadium titanomagnetite pellets (CVTP) with Cr₂O₃ addition were studied, and the reduction swelling index (RSI) and compressive strength (CS) of the reduced CVTP with simulated coke oven gas (COG) injection were investigated. The results showed that the CS of the CVTP decreases and the porosity of the CVTP increases with increasing amount of Cr₂O₃ added. The Cr₂O₃ mainly exists in the form of (Cr, Fe)₂O₃ solid solution in the CVTP and as Fe–Cr in the reduced CVTP. The CS of the reduced CVTP increases and the RSI of the reduced CVTP decreases with increasing amount of Cr₂O₃ added. The limited aggregation and diffusion of metallic iron contribute to the formation of dense lamellar crystals, which leads to the slight decrease for reduction swelling behavior of reduced CVTP. This work provides a theoretical and technical basis for the utilization of CVTP and other Cr-bearing ores such as chromite with COG recycling technology.

Keywords: chromium oxide; oxidation induration; reduction swellability; coke oven gas; chromium-bearing vanadium titanomagnetite pellets

1. Introduction

The blast furnace (BF) is widely used in the ironmaking process and the BF ironmaking has been the primary ironmaking method. Nevertheless, the massive utilization of coke and coal in the BF process generates large amounts of carbon monoxide (CO) and carbon dioxide (CO₂). The CO₂ emissions from the iron and steel industry are responsible for approximately 15% of the total CO₂ emissions in China [1]. At present, the amount of idle coke oven gas (COG) produced by the Baosteel Co., Ltd. is greater than 6.5×10^7 m³ per year. The average calorific value of COG is 18500 kJ/m³. Hence, COG represents a valuable fuel that could be used to decrease the consumption of coal and coke in BF. In addition, COG contains 60.7vol% H₂ and COG injection is recognized as a viable method to decrease CO₂ emissions and enable low-carbon ironmaking in BF. Mousa *et al.* [2] studied the influence of COG injection on a BF with isothermal and nonisothermal reduction of sinter under differ-

ent gas compositions and temperatures; they found that the reduction rate could be increased with COG injection under isothermal conditions. Liu *et al.* [3] speculated that COG injection into a BF could increase hot-metal productivity and decrease the coal ratio, coke ratio, and the carbon emissions of the BF. Wang *et al.* [4] conducted a mathematical simulation of BF operation with COG injection and found that the indirect reduction degree increases because of the involvement of hydrogen in the cohesive zone with COG injection. They further found that the productivity and utilization efficiency of CO increased and CO₂ emission and energy consumption decreased with COG injection. Nishioka *et al.* [5] considered that COG is a readily available and stable hydrogen source for industry. Meanwhile, COG has been successfully used in a BF in the COURSE50 project (CO₂ ultimate reduction in steelmaking process by innovative technology for cool earth 50). Mousa *et al.* [6] found that the reduction rate of pellets increased sharply with COG injection.

Corresponding authors: Song-tao Yang E-mail: yangsongtao1984@163.com; Xiang-xin Xue E-mail: xuexx@mail.neu.edu.cn

© University of Science and Technology Beijing and Springer-Verlag GmbH Germany, part of Springer Nature 2019

The chromium-bearing vanadium titanomagnetite (CVTM) in the Panzhihua, Sichuan province in China is a large reserve resource, and the reserves are more than 3.5 billion tons [7]. The CVTM is one of the largest vanadium titanomagnetite (VTM) mineral resources that includes V, Cr, and many other elements [8]. The grade of Cr in the Hongge mine is as high as 0.81wt%. Similar types of ores are mainly distributed in Russia, Canada, Australia, and other places in the world [9–10]. Many studies on the utilization of CVTM have been conducted, whereas studies on the reduction of chromium-bearing vanadium titanomagnetite pellets (CVTP) with COG are scarce [11–12]. Given the under-researched and preindustrial technology of CVTM in the BF process, studies of reduction of CVTP with COG injection are necessary. Cheng *et al.* [9] studied the effect of Cr₂O₃ on the reduction of high-chromium vanadium-titanium pellets. Their results showed that the Cr₂O₃ adversely affected the reduction process and increased the smelting difficulty of CVTP. Li *et al.* [13–14] investigated the effect of Cr₂O₃ on oxidation induration and reduction behavior of CVTP with simulated shaft furnace gases and found that the reduction swelling index (RSI) increases with increasing Cr₂O₃ addition because of the formation of metallic iron whiskers. The work was closely related to the smelting parameters on the separation behaviors of CVTP obtained from the gas-based direct reduction

process [15]. As noted in previous papers, the reduction of CVTM by COG has not been mentioned. Due to chromium is one of the main valuable elements in CVTM, investigations of its mechanism of influence in the oxidation and reduction process of CVTM by utilization of COG are warranted to supply the theoretical basis and technical support.

In the present study, the effects of Cr₂O₃ addition on the phase compositions, compressive strength (CS), porosity, microstructure, and oxidation induration of CVTP were analyzed. Furthermore, the effect of Cr₂O₃ addition on the reduction swelling behavior of reduced CVTP with simulated COG injection was investigated. The results provided theoretical and technical bases for the smelting of CVTP and other Cr-bearing minerals such as chromite with COG recycling technology.

2. Experimental

2.1. Materials

The CVTM was obtained from Hongge (Sichuan, China). The chemical compositions of the CVTM and bentonite are listed in Table 1. Fig. 1 shows the X-ray diffraction (XRD) pattern of the CVTM. The main minerals of the CVTM are Fe₃O₄ and FeTiO₃. The Cr₂O₃ was analytical grade and was purchased from Sinopharm Chemical Reagent Co. (China).

Table 1. Chemical compositions of raw materials

wt%

Materials	Fe _{Total}	FeO	TiO ₂	Co ₂ O ₃	V ₂ O ₅	Cr ₂ O ₃	CaO	SiO ₂	MgO	Al ₂ O ₃	P	S
CVTM	53.35	26.91	11.60	0.02	0.57	0.81	0.96	4.71	3.33	2.82	0.02	0.26
Bentonite	—	—	—	—	—	—	2.19	68.28	3.56	13.45	—	—

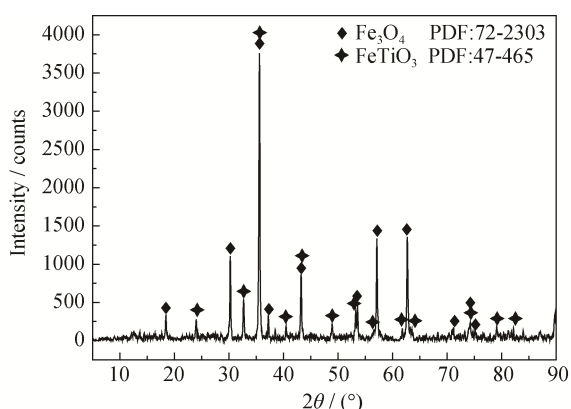


Fig. 1. XRD pattern of the CVTM.

2.2. Apparatus and procedure

The pelletizing process includes mixing, balling, drying, oxidation induration, and cooling. The main parameters of the pelletization process were 8.0wt% moisture of the mix-

ing materials, 1.0wt% of bentonite, 30 min of pelletizing time, 10–12 mm of green pellets, a drying temperature of 105°C for 5 h, a preheating temperature of 900°C for 20 min, and a roasting temperature of 1200°C for 20 min with 1.5 L/min blown air. When the oxidation process was finished, the CVTP was removed from the muffle furnace with the temperature lower than 900°C and allowed to cool to ambient temperature.

The reduction swelling behavior of the CVTP was studied in a comprehensive metallurgical measuring apparatus, as shown in Fig. 2. First, the 18 CVTP samples with an average size of 10–12.5 mm were placed into the constant-temperature zone of the apparatus and heated to the target temperature under the N₂ atmosphere flowing at 3 L/min. Then, COG injection (150 m³/t hot metal, 40vol%CO–15vol%H₂–10vol%CO₂–35vol%N₂) was purged into the apparatus at 15 L/min. Finally, the reactor was re-

moved from the apparatus and cooled in the N₂ atmosphere when the reduction was completed. The RSI and CS of reduced CVTP were measured. The reduction temperature and time were 900°C and 60 min, respectively.

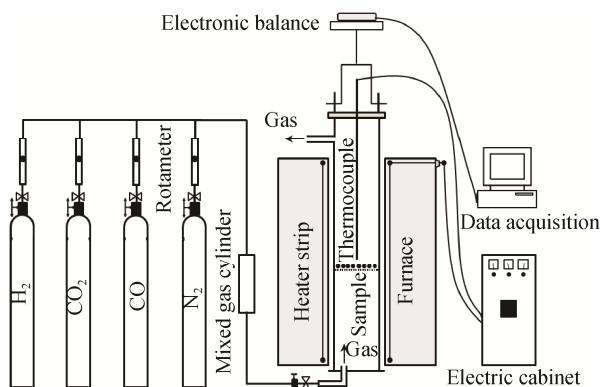


Fig. 2. Schematic of the experimental apparatus.

The RSI is defined as

$$\text{RSI} = \frac{V_t - V_0}{V_0} \times 100\% \quad (1)$$

where V_0 and V_t are the volumes of original CVTP and reduced CVTP, respectively, mm³. The diameters of the CVTP and reduced CVTP were measured with electronic Vernier calipers.

2.3. Analytical methods

X-ray fluorescence (XRF, ZSXPrimus II; Rigaku, Japan) was used to determine the chemical compositions of the raw materials. XRD (X'Pert Pro; PANalytical, Almelo, The Netherlands) with Cu K_α radiation (wavelength = 0.15406 nm) generated at 40 kV and 40 mA was used to analyze the mineral phases of the CVTM and CVTP. Scanning electron microscopy (SEM) conducted with an electron microscope (Ultra Plus; Carl Zeiss GmbH, Jena, Germany) equipped with a backscattering electron (BSE) detector and an energy-dispersive spectroscopy (EDS) apparatus was used to detect the microstructure of CVTP. The porosity and pore size distribution of CVTP were tested by mercury-injection porosimetry (Micromeritics Instrument Corp., Autopore IV 9500, USA). The CS of CVTP was measured according to standard ISO4700.

3. Results and discussion

3.1. Oxidation induration of CVTP

3.1.1. Phase composition

The oxidation induration process of CVTP includes a series of physicochemical reactions. Fig. 3 shows the primary

phases of CVTP with different Cr₂O₃ addition amounts. The XRD peak of Cr₂O₃ was not detected in all samples and the primary phases of CVTP with or without Cr₂O₃ addition are both Fe₂O₃, Fe₂TiO₅, and (Cr, Fe)₂O₃ solid solution; however, the peak position of the (Cr, Fe)₂O₃ solid solution shifted toward higher angles with increasing Cr₂O₃ addition amount, indicating that Cr₂O₃ dissolved into the hematite lattice to generate a solid solution. The main oxidation reactions and phase transformations of Fe₃O₄, FeTiO₃, and Cr₂O₃ in CVTP can be written as:

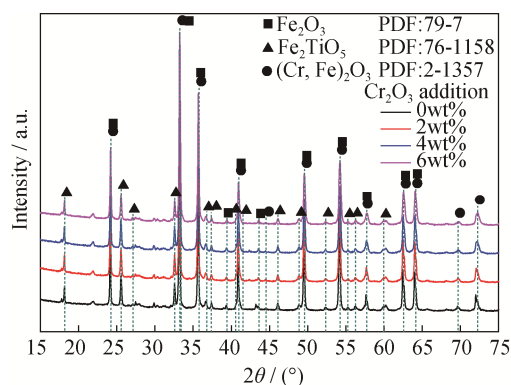
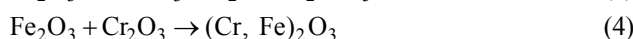


Fig. 3. XRD patterns of CVTP with different Cr₂O₃ additions.

3.1.2. Compressive strength and porosity

Fig. 4 shows the changes in CS and porosity of CVTP with different Cr₂O₃ additions. The CS clearly decreases from 2448 to 1891 N and the porosity increases from 14.86% to 19.84% with increasing Cr₂O₃ addition. Fig. 5 shows the relationship between the porosity and the CS; the porosity increases as the CS decreases. Furthermore, they exhibit a negative correlation relationship. The experimental linear regression equation between the porosity and the CS of CVTP is

$$C = -114.0P + 4124.36 \quad (5)$$

where the C is the CS and P is the porosity of the CVTP.

On the basis of the empirical equation between porosity and CS (Eq. (6)), where d is the grain radius (cm) and K , α , and η are coefficients[16], the CS really decreases with increasing porosity.

$$C = K \cdot d^{-\alpha} \cdot \exp(-\eta \cdot P) \quad (6)$$

Orowan [17] studied the equation of theoretical fracture strength of the solid material σ_{th} (Eq. (7)), where E is the elastic modulus, γ_s is the free surface energy, and r_0 is the mean radius of atoms.

$$\sigma_{th} = \sqrt{\frac{E\gamma_s}{r_0}} \quad (7)$$

Spriggs [18] studied the effect of porosity on the elastic modulus and deduced the following equation (Eq.(8)), where E_0 is the elastic modulus of the nonporous sample and β is an empirical constant.

$$E = E_0 \cdot \exp(-\beta \cdot P) \quad (8)$$

Hence, the relationship between theoretical fracture strength and porosity is

$$\sigma_{th} = \sqrt{\frac{E_0 \cdot \gamma_s}{r_0 \cdot \exp(\beta \cdot P)}} \quad (9)$$

According to Eq. (9), the theoretical fracture strength decreases exponentially with increasing porosity, which means that the theoretical fracture strength decreases with increasing number of pores in the pellets. Hence, with the addition of Cr_2O_3 , the porosity increases as the CS decreases.

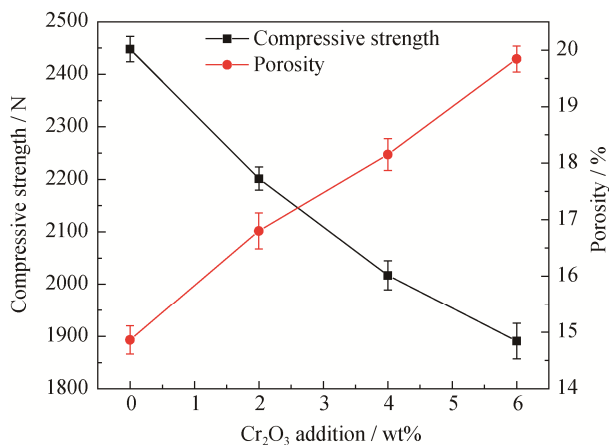


Fig. 4. Effect of Cr_2O_3 addition on the compressive strength and porosity of CVTP.

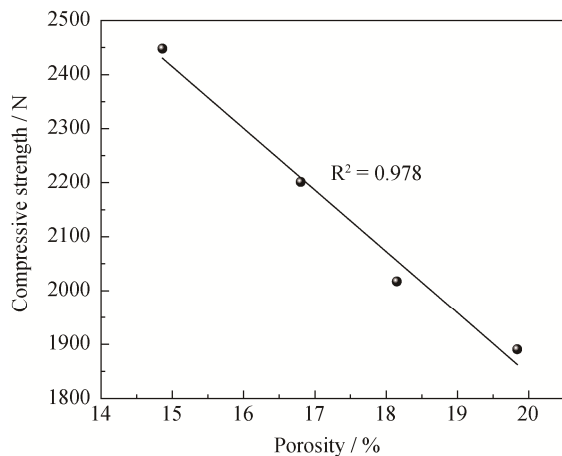


Fig. 5. Relationship between porosity and compressive strength of CVTP.

According to the histograms, Fig. 6 shows the effect of different Cr_2O_3 additions on the pore size distribution of CVTP in logarithmic form. The microsize pore size distribution of CVTP mainly distributes between 0 and 5 μm when the Cr_2O_3 addition amount is less than 4wt%. In addition, the proportion of micro-sized pores in the pore size distribution of CVTP clearly decreases with increasing Cr_2O_3 addition amount, as indicated by the incremental intrusion of mercury into micro-sized pores decreasing continuously. Meanwhile, the pore size increased markedly in a large range from 5 to 30 μm when Cr_2O_3 addition increased from 4wt% to 6wt%, which corresponds to an increase in porosity from 18.15% to 19.84%.

3.1.3. Microscopic structure

Fig. 7 shows the microstructure of CVTP with different Cr_2O_3 additions, as observed by SEM and Table 2 shows the EDS analysis result of points and phases in the Fig. 7. On the basis of the XRD analysis of CVTP with various Cr_2O_3 addition, the Cr_2O_3 mainly exists as a $(\text{Cr}, \text{Fe})_2\text{O}_3$ solid solution on the phase composition of CVTP during the oxidation induration process. As shown in Fig. 7(a), forsterite exists among the hematite, and the connection between the forsterite and hematite appears fragile; the forsterite mineral does not contain Cr. The foliated pseudobrookite exists in the hematite with distinct boundaries, and its Cr content is 1.19wt%. The gangue minerals exist at the boundaries and interiors of hematite, and some Cr dissolves into these gangue minerals, which connect with hematite. The contents of Cr in gangue mineral is 0.29wt%. Furthermore, the concentrations of Mg and Al in the gangue minerals (points 3 and 4) are high, and the existence of Mg^{2+} and Al^{3+} tends to impede the further oxidation of iron oxides. As shown in Figs. 7(b)–7(d), the Cr mainly exists in the intervals of hematite and reacts with hematite to form micropore-structured $(\text{Cr}, \text{Fe})_2\text{O}_3$ solid solution on the boundaries of hematite and then dissolves into the interior of the hematite. The content of Cr in the product layer (points 6, 9, and 12) between Cr_2O_3 and hematite clearly increases from 2.02wt% to 12.96wt% with increasing Cr_2O_3 addition amount, and the $(\text{Cr}, \text{Fe})_2\text{O}_3$ solid solution layer and the size of the micropores increase simultaneously. Moreover, Cr dissolves into the ilmenite. Zhu *et al.* [19] studied the oxidation of pellets prepared from a mixture of magnetite and chromite and observed substantial internal diffusion of Fe^{3+} from hematite to chromite spinel and counter-diffusion of Cr^{3+} and Al^{3+} from chromite spinel to outer hematite to form sesquioxide $(\text{Fe}, \text{Cr}, \text{Al})_2\text{O}_3$. Meanwhile, the $(\text{Cr}, \text{Fe})_2\text{O}_3$ solid solution is thermodynamically stable in the oxidation process. The generation

of (Cr, Fe)₂O₃ solid solution layer changes the morphology and impedes the recrystallization process of hematite, which

leads to a decrease of CS and an increase of porosity of CVTP.

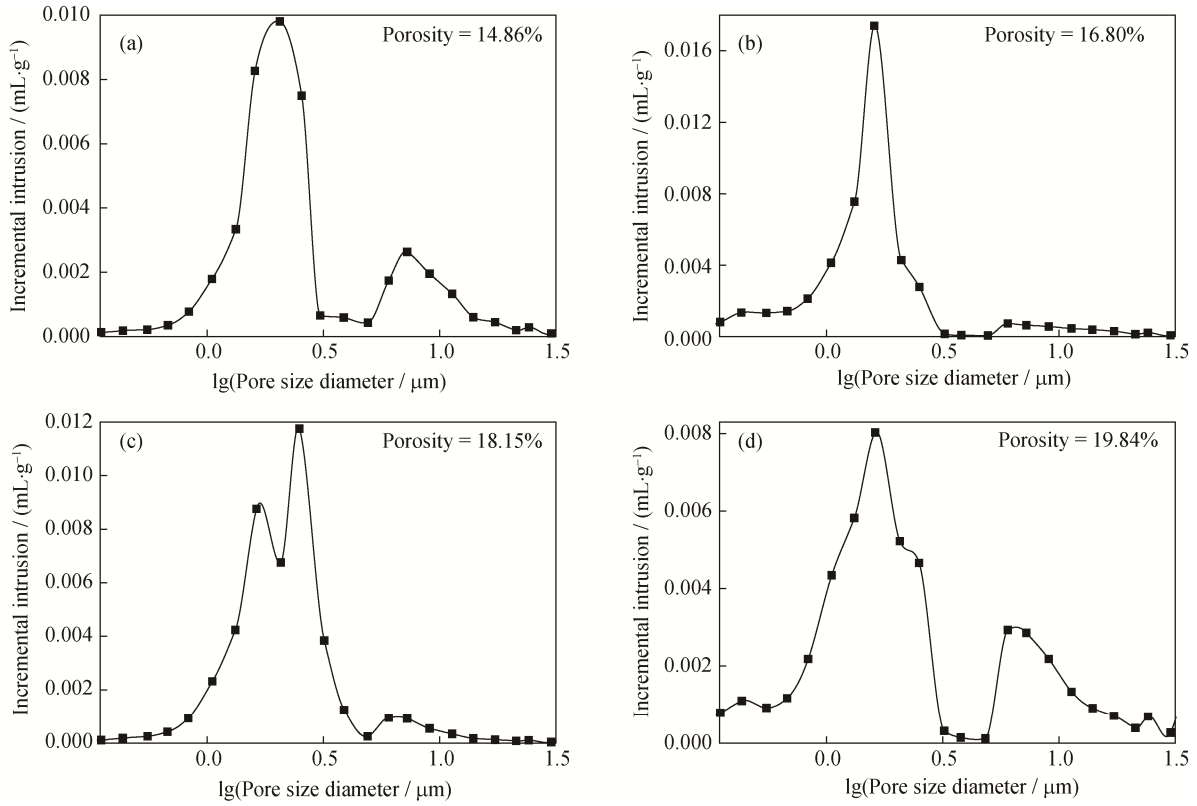


Fig. 6. Porosity and pore size distribution of CVTP with various Cr₂O₃ addition amounts: (a) 0wt%; (b) 2wt%; (c) 4wt%; (d) 6wt%.

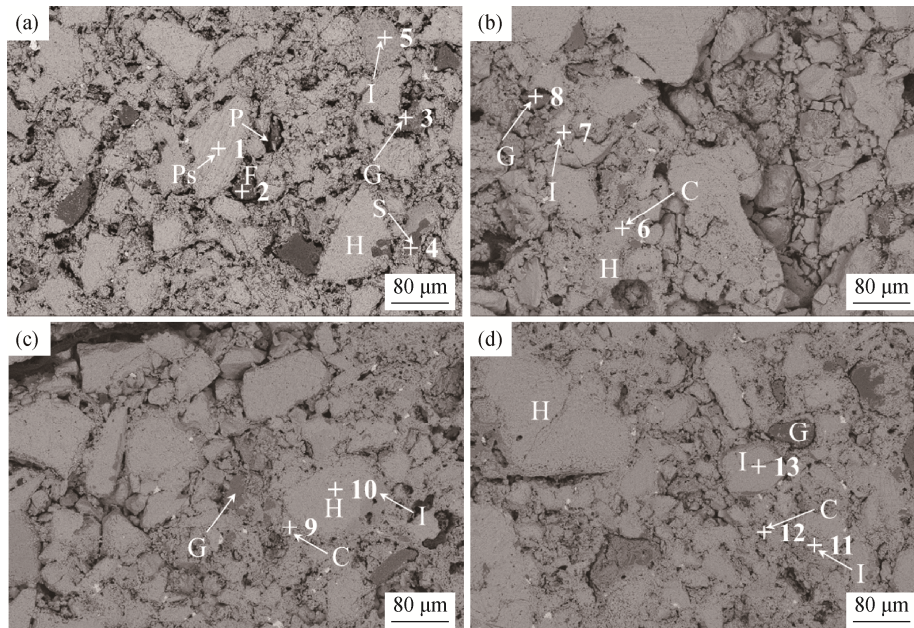


Fig. 7. SEM images and EDS analysis of CVTP with Cr₂O₃ different additions: (a) 0wt%; (b) 2wt%; (c) 4wt%; (d) 6wt%. H: hematite; C: (Cr, Fe)₂O₃ solid solution; I: ilmenite; Ps: pseudobrookite; F: forsterite; G: gangue; S: spinel; P: pore.

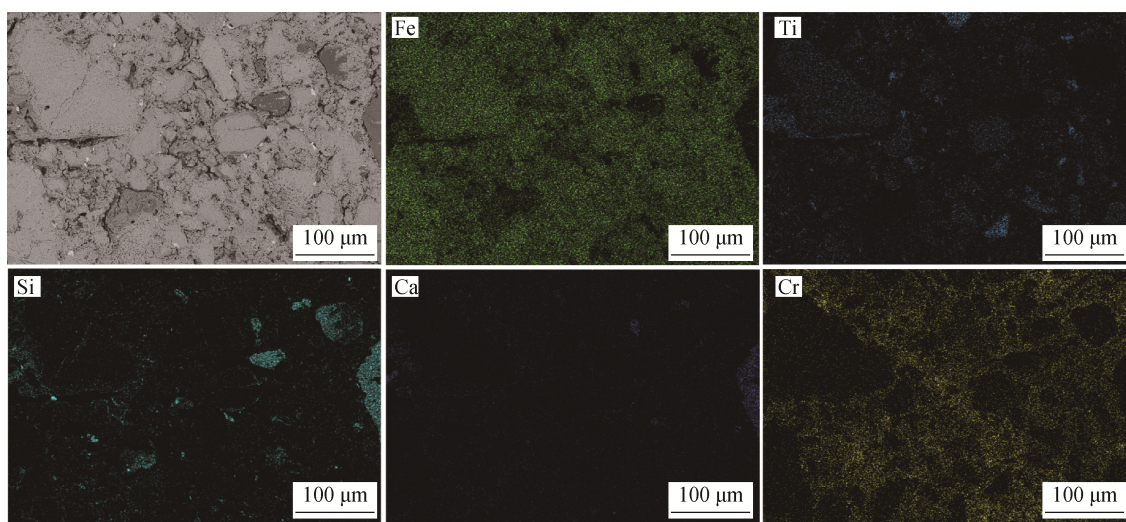
Table 2. EDS analysis result of points in Fig. 7

wt%

Points/Phases	Fe	Cr	Ti	V	Mg	Al	Si	Ca	O
1/Ps	66.25	1.19	2.85	0.15	0.23	0.67	0.00	0.04	27.97
2/F	5.80	0.00	0.29	1.74	20.72	0.70	30.02	3.22	36.47
3/G	6.78	0.29	0.47	1.41	7.31	12.69	21.17	8.69	35.76
4/S	18.45	1.84	0.42	0.13	12.13	35.06	0.01	0.08	31.40
5/I	40.42	0.00	26.36	0.38	0.14	0.13	0.13	0.12	31.46
6/C	61.96	2.02	6.92	0.23	1.79	1.29	0.00	0.05	25.09
7/I	39.82	1.08	26.26	0.72	2.24	1.25	2.68	0.49	24.85
8/G	1.90	0.04	0.26	1.24	0.27	2.11	45.85	1.66	46.60
9/C	53.95	5.33	4.09	0.55	1.35	2.71	2.45	1.66	27.28
10/H	67.80	0.16	4.64	0.20	1.46	1.41	0.02	0.00	23.38
11/I	37.88	1.18	22.47	0.67	1.12	0.55	4.02	0.21	31.05
12/C	43.85	12.96	3.04	0.56	1.74	1.28	0.78	0.60	34.72
13/I	47.82	0.57	18.00	0.66	0.75	0.36	0.05	0.04	31.12

The induration of pellets greatly depends on the solid-state bonding. Friel and Erickson [20] considered that the bonding of magnetite pellets is primarily oxide induration when the basicity of the pellets is less than 0.8. Nevertheless, bentonite is usually added during the pelleting process as a binder, and the liquid phase will induce oxidation induration because the bentonite contains siliceous gangue. The formed liquid phases fill the intervals among mineral particles. The liquid phases can connect mineral

particles, promote particle rearrangement, and accelerate ion exchange among mineral particles. As shown in Fig. 8, a siliceous liquid phase can be obtained in CVTP. The siliceous liquid phase distributes in the gaps of mineral particles and a $(Cr, Fe)_2O_3$ solid solution with an incompact and porous structure, improving the induration and intensity of pellets; however, the degree of influence of the siliceous liquid phase is low in comparison to the effect of $(Cr, Fe)_2O_3$ solid solution.

Fig. 8. X-ray element mapping of CVTP with 6wt% Cr_2O_3 addition.

3.1.4 Induration mechanism

According to the aforementioned results, the Cr_2O_3 addition has an inhibiting effect on the recrystallization of hematite grains, changes the morphology of hematite boundaries, and strengthens the loose structure in the intervals of hematite grains because of the generation of $(Cr, Fe)_2O_3$ solid so-

lution. Fig. 9 shows the schematic diagrams of oxidation induration mechanism of CVTP. The hematite grains are large-grained and interconnected and distribute relatively uniformly in the absence of Cr_2O_3 addition. Furthermore, the hematite grains fully recrystallize and connect and bonding phases exist at the intervals of grains; both of these

effects enhance the CS of the CVTP. Nevertheless, the loose and porous (Cr, Fe)₂O₃ solid solution fills the intervals of hematite grains when Cr₂O₃ is added. The Cr₂O₃ mainly reacts with hematite to generate (Cr, Fe)₂O₃ at the boundaries of the hematite. The (Cr, Fe)₂O₃ solid solution increases the porous structure and decreases recrystallization of the hematite grains. Hence, Cr₂O₃ addition is disadvantageous to the oxidation induration of the CVTP and decreases its CS.

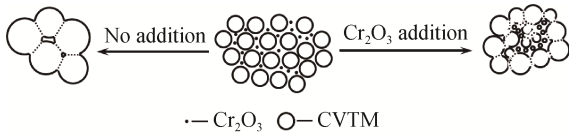


Fig. 9. Schematic of the oxidation induration mechanism of CVTP with Cr₂O₃ addition.

3.2. Swelling behavior of CVTP

3.2.1. Phase composition

Fig. 10 shows the XRD patterns of reduced CVTP with different Cr₂O₃ additions, after reduction for 60 min. The XRD patterns show a gradual change in peak positions with Cr₂O₃ addition, indicating that the addition of Cr₂O₃ affects the phase composition of reduced CVTP. The primary phases of reduced CVTP are Fe, FeO, Fe₂TiO₄, and Fe–Cr. Liu *et al.* [21] reported that the Fe₂TiO₄ is one of the reduction products of iron titanium reduced with H₂. Meanwhile, the peak intensity of Fe₂TiO₄ clearly increases with increasing Cr₂O₃ addition as shown in the Fig. 10. On the one hand, the H₂ accelerates the reduction of iron oxides. On the other hand, the increasing porosity of CVTP enhances the reduction rate of the pellets.

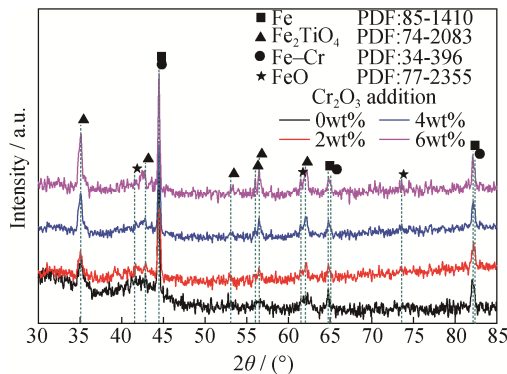


Fig. 10. XRD patterns of reduced CVTP with different Cr₂O₃ additions.

In the reduction of CVTP with simulated COG injection, the main possible reactions can be classified as the reduction of Fe₂O₃, Fe₂TiO₅, and (Cr, Fe)₂O₃ solid solution and side reactions of the products. The possible chemical reactions

during the reduction of CVTP with simulated COG injection are expressed in Table 3. Reactions (10)–(13) and Reactions (16)–(19) are the possible reduction reactions of hematite by CO and H₂, respectively. Reaction (14) and Reaction (20) are the possible reduction reactions of Fe₂TiO₅, respectively. Fig. 11 shows the relation between ΔG[⊖] and T for the possible CVTP reduction reactions. According to the calculation results, the whole ΔG[⊖] lines of Reactions (14) and (19) are below the zero line, which means that the Fe₂TiO₅ can be reduced to Fe₂TiO₄ by both CO and H₂ at a reduction temperature of 900°C. Furthermore, Reaction (15) and Reaction (21) are the possible reduction reactions of (Cr, Fe)₂O₃ by CO and H₂, respectively.

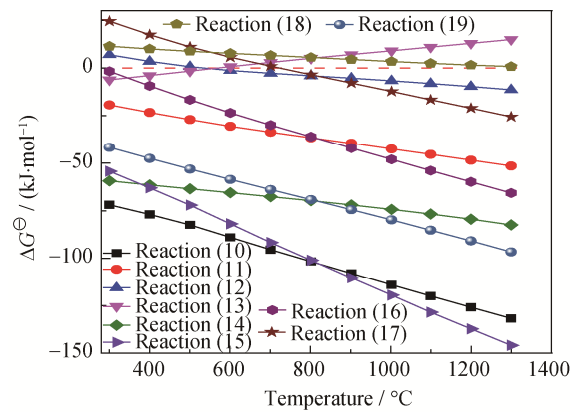


Fig. 11. Relation between ΔG[⊖] and T for CVTP possible reduction reactions.

Table 3. Reduction reactions of CVTP

Reactions	Numbers
3Fe ₂ O ₃ + CO = 2Fe ₃ O ₄ + CO ₂	(10)
Fe ₂ O ₃ + CO = 2FeO + CO ₂	(11)
Fe ₃ O ₄ + CO = 3FeO + CO ₂	(12)
FeO + CO = Fe + CO ₂	(13)
Fe ₂ TiO ₅ + CO = Fe ₂ TiO ₄ + CO ₂	(14)
(Cr, Fe) ₂ O ₃ + 3CO = 2(Fe–Cr) + 3CO ₂	(15)
3Fe ₂ O ₃ + H ₂ = 2Fe ₃ O ₄ + H ₂ O	(16)
Fe ₂ O ₃ + H ₂ = 2FeO + H ₂ O	(17)
Fe ₃ O ₄ + H ₂ = 3FeO + H ₂ O	(18)
FeO + H ₂ = Fe + H ₂ O	(19)
Fe ₂ TiO ₅ + H ₂ = Fe ₂ TiO ₄ + H ₂ O	(20)
(Cr, Fe) ₂ O ₃ + 3H ₂ = 2(Fe–Cr) + 3H ₂ O	(21)

3.2.2. Effect of time and Cr₂O₃ addition on RSI

The physical stability of CVTP in BF is an important factor in the reduction process. The RSI and CS are the important physical characteristics of reduced CVTP. The swelling behavior with simulated COG injection into BF at 900°C as a function of time was studied; the results are

shown in Fig. 12. Fig. 12 shows the different reduction stages in the swelling behavior of reduced CVTP. The RSI of reduced CVTP can be separated into three stages: the initial stage, intermediate stage, and final stage. In the initial stage, the RSI increases rapidly with increasing time and reaches the peak value of 8.45% at 15 min. Moreover, the RSI decreases gradually in the intermediate stage with increasing time. Furthermore, the RSI decreases relaxedly as a smooth curve in the final stage with increasing time. Finally, the RSI reaches 5.87% at 60 min. The intermediate stage and final stage indicate the CVTP shrinks after 15 min, which is speculated to be the sintering of iron whiskers and grains. Hence, the maximum swelling of CVTP occurs at 15 min at a reduction temperature of 900°C. Sharma *et al.* [22] investigated possible causes of the shrinkage, including the sintering of iron whiskers and pores and the formation of silicate phases. These phenomena restrict the growth and crystallization of iron whiskers in the structure of reduced pellets and result in shrinkage of the pellets.

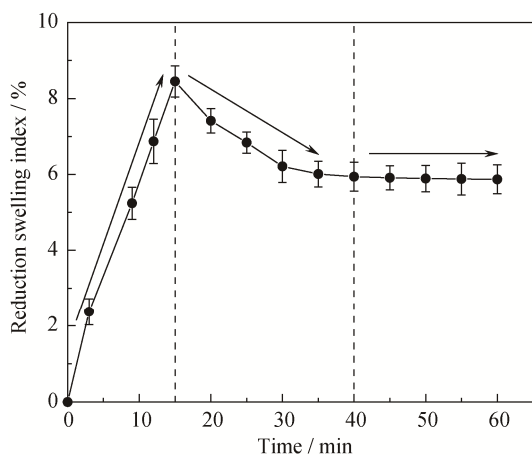


Fig. 12. Effect of time on the reduction swelling index of reduced CVTP without Cr₂O₃ addition.

Fig. 13 shows the effect of Cr₂O₃ addition on the RSI and CS of reduced CVTP with simulated COG injection into BF. The RSI decreases from 5.87% to 3.25%, whereas the CS increases from 901 to 1036 N with increasing Cr₂O₃ addition from 0wt% to 6wt%. Sharma *et al.* [23] studied the effect of oxidation induration on the reduction swelling behavior of pellets and found that an increase in the CS and decrease of the porosity of pellets result in a decrease of the RSI. Hence, the CS and porosity of pellets influence the RSI of pellets. The low reduction swelling of pellets is mainly caused by the presence of slag bonds, which cannot push the adjacent grains mechanically and lead to a decrease of volume [24]. Moreover, the generation of iron whiskers during reduction leads to additional stresses in pellets, a higher CS

of reduced CVTP, and less reduction swelling of CVTP. In previous studies, the reduction swelling of pellets usually reached a maximum value at approximately 900°C for reduction carried out with CO in the temperature range 800–1100°C because of the formation of a mass of whiskers at approximately 900°C [25]. Yi *et al.* [26] investigated the effect of adding H₂ to the reduction atmosphere and observed decreased swelling and expansion characteristics of pellets, which indicated a higher CS of reduced CVTP, because the pellets passed the wüstite stage rapidly and the bonding of the reduced pellets was remarkably improved.

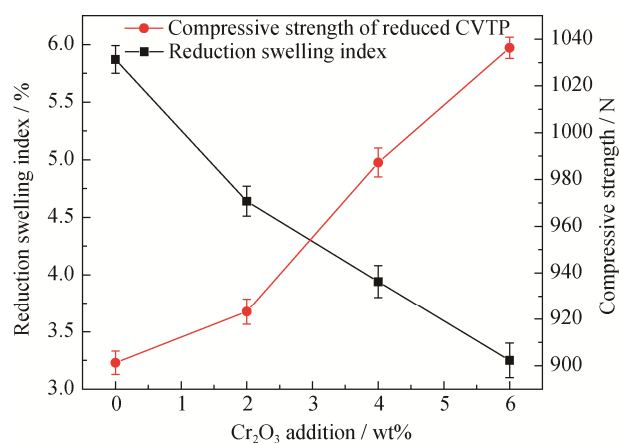


Fig. 13. Effect of Cr₂O₃ addition on the reduction swelling index and compressive strength of reduced CVTP.

3.2.3. Microscopic structure

To reveal the mechanism of swelling behavior and CS of reduced CVTP, the microstructures of reduced CVTP with different Cr₂O₃ additions were detected; the results are shown in Fig. 14. The results indicate that the Cr₂O₃ addition prominently affects the microstructures of the reduced CVTP. As shown in Fig. 14(a), the microstructure of reduced CVTP is reticular and filiform, and metallic iron whiskers exist in the reticular structure. Hence, the generation of metallic iron whiskers results in the reticular structure and reduction swelling of CVTP. Fig. 14(b) shows that the metallic iron whiskers form on the surfaces of lamellar grains as the cellular structure forms when the Cr₂O₃ addition amount is 2wt%. The lamellar microstructure of CVTP with 2wt% Cr₂O₃ is thin. When the Cr₂O₃ addition amount is increased to 4wt%, the metallic iron whiskers grow gradually, the interval among lamellar crystals shrinks, and some metallic iron particles aggregate at the intervals. Additionally, the reduction swelling of CVTP decreases further when the Cr₂O₃ addition is increased to 6wt%, as shown in Fig. 13. Fig. 14(d) shows that the lamellar grains are denser than those formed with low Cr₂O₃ additions of CVTP. The inter-

vals of lamellar grains are small, and the cracks also become less abundant and smaller. Hence, the RSI of the reduced CVTP decreases gradually with increasing Cr₂O₃ addition, as shown in Fig. 13.

On the basis of the aforementioned analysis, Fig. 15 shows the evolutive schematics of the reduction swelling behavior of reduced CVTP with Cr₂O₃ addition during the reduction process with simulated COG injection. The round dot of metallic iron decreases, and the dense interval of lamellar crystals form with high Cr₂O₃ addition. Under these

conditions, the CS of the reduced CVTP is high and the RSI of the reduced CVTP is low, with little reduction swelling. When large amount of Cr₂O₃ are added, the limited aggregation and diffusion of metallic iron contribute the dense lamellar crystals, leading to little reduction swelling. Hence, the addition of Cr₂O₃ decreases the reduction swelling of CVTP and improves the CS of CVTP. Wang and Sohn [25] studied the reduction swelling behavior of iron ore during the reduction process and deduced that the metal iron whiskers were a critical factor that caused the swelling.

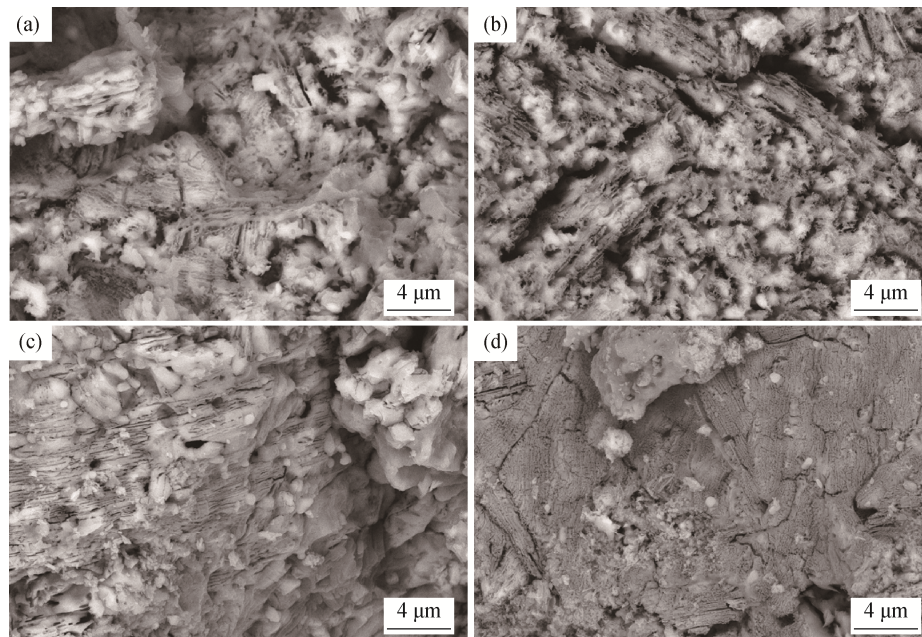


Fig. 14. SEM images of reduced CVTP with Cr₂O₃ additions (a) 0wt%; (b) 2wt%; (c) 4wt%; and (d) 6wt%.



Fig. 15. Schematics of the swelling behavior of reduced CVTP with Cr₂O₃ addition.

4. Conclusions

(1) The primary phases of CVTP with Cr₂O₃ addition are Fe₂O₃, Fe₂TiO₅, and (Cr, Fe)₂O₃ solid solution. The CS of the CVTP decreases from 2448 to 1891 N and its porosity increases from 14.86% to 19.84% with increasing Cr₂O₃ addition from 0wt% to 6wt%.

(2) The generation of the (Cr, Fe)₂O₃ solid solution layer changes the morphology and impedes the recrystallization process of hematite, leading to a decrease of the CS and an increase of the porosity of the CVTP.

(3) The primary phases of the reduced CVTP with simulated COG injection are Fe, FeO, Fe₂TiO₄, and Fe–Cr. The

RSI of the reduced CVTP without Cr₂O₃ addition increases rapidly with increasing time, reaching the peak value of 8.45% at 15 min, and then decreases to 5.87% smoothly with increasing time.

(4) The RSI decreases from 5.87% to 3.25%, whereas the CS of reduced CVTP increases from 901 to 1036 N with increasing Cr₂O₃ addition. The Cr₂O₃ addition decreases the reduction swelling of CVTP and improves the CS of reduced CVTP.

Acknowledgements

This research was financially supported by the National Natural Science Foundation of China (Nos. 51674084, 51174051, and 51574082).

References

- [1] X.C. Tan, H. Li, J.X. Guo, B.H. Gu, and Y. Zeng, Ener-

- gy-saving and emission-reduction technology selection and CO₂ emission reduction potential of china's iron and steel industry under energy substitution policy, *J. Cleaner Prod.*, 222(2019), p. 823.
- [2] E.A. Mousa, A. Babich, and D. Senk, Enhancement of iron ore sinter reducibility through coke oven gas injection into the modern blast furnace, *ISIJ Int.*, 53(2013), No. 8, p. 1372.
- [3] Z.G. Liu, M.S. Chu, T. Guo, H.T. Wang, and X. Fu, Numerical simulation on novel blast furnace operation of combining coke oven gas injection with hot burden charging, *Ironmaking Steelmaking*, 43(2016), No. 1, p. 64.
- [4] H.T. Wang, M.S. Chu, T.L. Guo, W. Zhao, C. Feng, Z.G. Liu, and J. Tang, Mathematical simulation on blast furnace operation of coke oven gas injection in combination with top gas recycling, *Steel Res. Int.*, 87(2016), No. 5, p. 539.
- [5] K. Nishioka, Y. Ujisawa, S. Tonomura, N. Ishiwata, and P. Sikstrom, Sustainable aspects of CO₂ ultimate reduction in the steelmaking process (COURSE50 Project), Part 1: Hydrogen reduction in the blast furnace, *J. Sustainable Metall.*, 2(2016), No. 3, p. 200.
- [6] E.A. Mousa, A. Babich, and D. Senk, Reduction behavior of iron ore pellets with simulated coke oven gas and natural gas, *Steel Res. Int.*, 84(2013), No. 11, p. 1085.
- [7] J. Tang, M.S. Chu, C. Feng, F. Li, Y.T. Tang, and Z.G. Liu, Coupled effect of valuable components in high-chromium vanadium-bearing titanomagnetite during oxidation roasting, *ISIJ Int.*, 56(2016), No. 8, p. 1342.
- [8] G.J. Cheng, Z.X. Gao, H. Yang, and X.X. Xue, Effect of diboron trioxide on the crushing strength and smelting mechanism of high-chromium vanadium-titanium magnetite pellets, *Int. J. Miner. Metall. Mater.*, 24(2017), No. 11, p. 1228.
- [9] G.J. Cheng, X.X. Xue, Z.X. Gao, T. Jiang, H. Yang, and P.N. Duan, Effect of Cr₂O₃ on the reduction and smelting mechanism of high-chromium vanadium-titanium magnetite pellets, *ISIJ Int.*, 56(2016), No. 11, p. 1938.
- [10] B.C. Jena, W. Dresler, and I.G. Reilly, Extraction of titanium, vanadium and iron from titanomagnetite deposits at pipestone lake, Manitoba, Canada, *Miner. Eng.*, 8(1995), No. 1-2, p. 159.
- [11] G.J. Cheng, Z.X. Gao, H. Yang, and X.X. Xue, Effect of calcium oxide on the crushing strength, reduction, and smelting performance of high-chromium vanadium-titanium magnetite pellets, *Metals*, 7(2017), No. 5, p. 181.
- [12] G.J. Cheng, X.X. Xue, T. Jiang, and P.N. Duan, Effect of TiO₂ on the crushing strength and smelting mechanism of high-chromium vanadium-titanium magnetite pellets, *Metall. Mater. Trans. B*, 47(2016), No. 3, p. 1713.
- [13] W. Li, G.Q. Fu, M.S. Chu, and M.Y. Zhu, Influence of Cr₂O₃ gas-based direct reduction behavior of Hongge vanadium titanomagnetite pellet with simulated shaft furnace gases, *ISIJ Int.*, 58(2018), No. 4, p. 604.
- [14] W. Li, N. Wang, G. Fu, M.S. Chu, and M.Y. Zhu, Effect of Cr₂O₃ addition on the oxidation induration mechanism of Hongge vanadium titanomagnetite pellet, *Int. J. Miner. Metall. Mater.*, 25(2018), No. 4, p. 391.
- [15] C. Feng, M.S. Chu, J. Tang, and Z.G. Liu, Effects of smelting parameters on the slag/metal separation behaviors of Hongge vanadium-bearing titanomagnetite metallized pellets obtained from the gas-based direct reduction process, *Int. J. Miner. Metall. Mater.*, 25(2018), No. 6, p. 609.
- [16] Y.M. Zhang, *Pellet Production Technology*, The Metallurgy Industry Press, Beijing, 2005, p. 67.
- [17] E. Orowan, Fracture and strength of solids, *Rep. Prog. Phys.*, 12(1949), No. 1, p. 185.
- [18] R.M. Spriggs, Expression for effect of porosity on elastic modulus of polycrystalline refractory materials, particularly aluminum oxide, *J. Am. Ceram. Soc.*, 44(1961), No. 12, p. 628.
- [19] D.Q. Zhu, C.C. Yang, J. Pan, Q. Zhang, B.J. Shi, and F. Zhang, Insight into the consolidation mechanism of oxidized pellets made from the mixture of magnetite and chromite concentrates, *Metall. Mater. Trans. B*, 47(2016), No. 2, p. 1010.
- [20] J.J. Friel and E.S. Erickson, Chemistry, microstructure, and reduction characteristics of dolomite-fluxed magnetite pellets, *Metall. Trans. B*, 11(1980), No. 2, p. 233.
- [21] Y.C. Liu, S. Nachimuthu, Y.C. Chuang, Y. Ku, and J.C. Jiang, Reduction mechanism of iron titanium based oxygen carriers with H₂ for chemical looping applications—a combined experimental and theoretical study, *RSC Adv.*, 6(2016), No. 108, p. 106340.
- [22] T. Sharma, R.C. Gupta, and B. Prakash, Effect of firing condition and ingredients on the swelling behaviour of iron ore pellets, *ISIJ Int.*, 33(1993), No. 4, p. 446.
- [23] T. Sharma, R.C. Gupta, and B. Prakash, Swelling of iron ore pellets by statistical design of experiment, *ISIJ Int.*, 32(1992), No. 12, p. 1268.
- [24] C.E. Seaton, J.S. Foster, and J. Velasco, Structural changes occurring during reduction of hematite and magnetite pellets containing coal char, *Trans. Iron Steel Inst. Jpn.*, 23(1983), No. 6, p. 497.
- [25] H.T. Wang and H.Y. Sohn, Effects of firing and reduction conditions on swelling and iron whisker formation during the reduction of iron oxide compact, *ISIJ Int.*, 51(2011), No. 6, p. 906.
- [26] L.Y. Yi, Z.C. Huang, T. Jiang, L.N. Wang, and T. Qi, Swelling behavior of iron ore pellet reduced by H₂-CO mixtures, *Powder Technol.*, 269(2015), p. 290.